HOKKAIDO UNIVERSITY

Title	Resonant acoustic-phonon modes in a quantum wire
Author(s)	Nishiguchi, Norihiko
Citation	Physical Review B, 52(7), 5279-5288 https://doi.org/10.1103/PhysRevB.52.5279
Issue Date	1995-08-15
Doc URL	https://hdl.handle.net/2115/47083
Rights	© 1995 The American Physical Society
Type	journal article
File Information	PhysRevB.52.5279.pdf

Hokkaido University Collection of Scholarly and Academic Papers : HUSCAP

Resonant acoustic-phonon modes in a quantum wire

Norihiko Nishiguchi
Department of Engineering Science, Hokkaido University, Sapporo 060, Japan
(Received 25 January 1995; revised manuscript received 27 April 1995)

We study the extended acoustic-phonon modes in a cylindrical GaAs quantum wire embedded in bulk AlAs. There are two kinds of resonant acoustic-phonon modes related to the wire dimensions: one is entirely extended in the system and the other is almost confined in the wire. Displacement of extended phonon modes in the wire region is enhanced for the resonant modes. The dispersion relations of these resonant modes have subband structures similar to those of confined phonon modes in free-standing wires. Owing to the resonant modes, the extended phonon modes, in the wire region, have characters of confined phonon modes in a free-standing wire rather than the usual bulk phonon modes.

I. INTRODUCTION

Transport phenomena of carriers confined in quasi-one-dimensional (Q1D) quantum wires have been extensively studied experimentally[1–3] and theoretically,[4–18] because of the possible high electron mobility[19] owing to the dimensional carrier confinement. The Q1D wire structures modify not only electronic states, but also phonon modes. It is known that, in an embedded quantum wire within another material (e.g., a GaAs wire surrounded by AlAs), there are two kinds of optical phonon modes referred to as confined and excluded optical phonon modes.[20–28] In addition to these optical phonon modes, the interface optical phonon modes[23–25] exist at the wire-surrounding interface and contribute to electron scattering[26–28] as do the confined optical phonons.

In contrast to the optical phonons, acoustic phonons were assumed to be the usual bulk acoustic phonons with a three-dimensional (3D) bulk character in the studies of electron-acoustic-phonon scattering, except in a free-standing wire,[29,30] although the acoustic-phonon modes were expected to be modified due to the Q1D wire structures as well. In a previous paper,[31] the present author analytically showed the existence of two kinds of acoustic-phonon modes, confined and interface acoustic-phonon modes, bound to a cylindrical quantum wire surrounded by another material. The Q1D wire structures will also modify extended acoustic-phonon modes. The extended acoustic-phonon modes are coupled modes of longitudinal (LA) and transverse acoustic (TA) waves, due to the Q1D wire structures, as well as the confined and interface phonon modes,[31] and resonant phonon modes related to the wire dimensions are expected to appear. The resonant phonon modes will modulate displacement in the wire region. As a result, the electron-acoustic-phonon couplings are changed, which will affect electron scattering. Thus, the modifications in the extended phonon modes are expected to cause further modifications in related carrier transport phenomena. The extended acoustic-phonon modes of the Q1D wires and their resonant modes have not been examined yet. In this paper, we analytically investigate the extended acoustic-phonon modes of a quantum wire embedded within another bulk material and make clear the resonant acoustic-phonon modes in the Q1D wire-surrounding systems.

The plan of this paper is as follows. In Sec. II, we give a model for a quantum wire embedded within another material and formalism based upon the potential theory. Extended phonon modes are classified into the three kinds of modes, due to the rotational symmetry of the modes. We investigate each phonon mode and its resonant modes in respective subsections of Sec. III. We also examine the density of states of these phonon modes in this section. A summary and discussion are given in Sec. IV.

II. MODEL AND FORMALISM

We consider a GaAs cylindrical wire of radius R surrounded by bulk AlAs. We assume isotropic elastic properties for both the materials, for simplicity, redefining the stiffness constants $C_{\alpha,12}$'s by $C_{\alpha,12} = C_{\alpha,11} - 2C_{\alpha,44}$. Here, α stands for GaAs (A) and AlAs (B). The stiffness constants used in this paper are $C_{\mathrm{GaAs},11} = 1.188 \times 10^{12}$ dyn cm^{-2}, $C_{\mathrm{GaAs},44} = 0.594 \times 10^{12}$ dyn cm^{-2} for GaAs and $C_{\mathrm{AlAs},11} = 1.202 \times 10^{12}$ dyn cm^{-2}, $C_{\mathrm{AlAs},44} = 0.589 \times 10^{12}$ dyn cm^{-2} for AlAs. The wire axis is taken as the z direction and the following calculations are performed in cylindrical coordinates (r, ϕ, z). Figure 1 shows the geometry of the quantum wire-surrounding system. Since the isotropic stiffness matrix has the same form in cylindrical and rectangular coordinates, the matrix elements are converted to abbreviated subscript notation by the relations $1 = rr$, $2 = \phi\phi$, $3 = zz$, $4 = z\phi$, $5 = rz$, $6 = r\phi$. The displacement vector $\mathbf{u}_\alpha$ is expressed in terms of the scalar potential $\phi_{\alpha 0}$ and two vector potentials $\mathbf{\Psi}_{\alpha 1}$ and $\mathbf{\Psi}_{\alpha 2}$ as

$$\mathbf{u}_\alpha = \nabla\phi_{\alpha 0} + \nabla \times \mathbf{\Psi}_{\alpha 1} + \nabla \times \nabla \times \mathbf{\Psi}_{\alpha 2}. \quad (1)$$

The vector potentials $\mathbf{\Psi}_{\alpha j}$ ($j = 1$ and 2) are given by $\mathbf{\Psi}_{\alpha j} = \mathbf{e}_z \phi_{\alpha j}$ ($j = 1$ and 2), where $\mathbf{e}_z$ denotes the unit

 ©1995 The American Physical Society

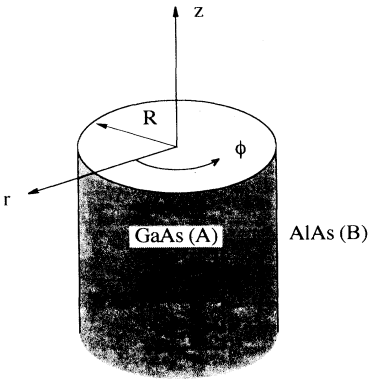

FIG. 1. Geometry of a cylindrical GaAs quantum wire surrounded by bulk AlAs.

vector of the z direction. The potential functions $\phi_{\alpha j}$ are readily known to obey the following scalar wave equation, substituting Eq. (1) into the wave equation for isotropic media, as

$$\rho_\alpha \frac{\partial^2 \phi_{\alpha j}}{\partial t^2} = [\delta_{j,0}\,(C_{\alpha,11} - C_{\alpha,44}) + C_{\alpha,44}]\,\nabla^2 \phi_{\alpha j}, \quad (2)$$

where ρ_α denotes the mass densities of GaAs ($5.36\ \mathrm{g\,cm^{-3}}$) and of AlAs ($3.76\ \mathrm{g\,cm^{-3}}$), and $\delta_{i,j}$ is the Kronecker symbol. The solution of Eq. (2) has the following form:

$$\phi_{\alpha j}(\mathbf{r}) = f_{\alpha j}(r) \exp[i(qz - \omega t + n\phi)], \quad (3)$$

where n is an integer denoting the n-fold rotational symmetry of the function about the wire axis, q the wave vector in the longitudinal direction, and ω an angular frequency.

Substituting Eq. (3) into (2), we obtain the following differential equation for $f_{\alpha j}$ as

$$\left(\frac{\partial^2}{\partial r^2} + \frac{1}{r}\frac{\partial}{\partial r} - \frac{n^2}{r^2} - q^2 + \frac{\omega^2}{v_{\alpha,j}^2}\right) f_{\alpha j}(r) = 0. \quad (4)$$

Here, $v_{\alpha,j}$ denotes the sound velocities of the bulk-LA and -TA waves given by

$$v_{\alpha,0} = v_{\alpha,\mathrm{LA}} = (C_{\alpha,11}/\rho_\alpha)^{1/2}, \quad (5a)$$

$$v_{\alpha,1} = v_{\alpha,2} = v_{\alpha,\mathrm{TA}} = (C_{\alpha,44}/\rho_\alpha)^{1/2}, \quad (5b)$$

respectively. The sound velocities are $v_{\mathrm{GaAs,LA}} = 4.708 \times 10^5\ \mathrm{cm\,sec^{-1}}$, $v_{\mathrm{GaAs,TA}} = 3.329 \times 10^5\ \mathrm{cm\,sec^{-1}}$, $v_{\mathrm{AlAs,LA}} = 5.654 \times 10^5\ \mathrm{cm\,sec^{-1}}$, and $v_{\mathrm{AlAs,TA}} = 3.958 \times 10^5\ \mathrm{cm\,sec^{-1}}$. Because $v_{\mathrm{AlAs,LA}} > v_{\mathrm{GaAs,LA}} > v_{\mathrm{AlAs,TA}} > v_{\mathrm{GaAs,TA}}$, the longitudinal wave number q of extended phonon modes must be smaller than $\omega/v_{\mathrm{AlAs,\,TA}}$. In this region, Eq. (4) yields a Bessel or modified Bessel equation for $f_{\alpha 0}$, depending on q, and a Bessel equation for $f_{\alpha 1}$ and $f_{\alpha 2}$. Within the wire, the finite potential functions ϕ_{Aj} are given by

$$\phi_{A0}(\mathbf{r},t) = \chi_{A0}\,\psi_{A0}(r) \exp[i(qz - \omega t + n\phi)], \quad (6a)$$

$$\phi_{A1}(\mathbf{r},t) = \chi_{A1}\,\psi_{A1}(r) \exp[i(qz - \omega t + n\phi)], \quad (6b)$$

$$\phi_{A2}(\mathbf{r},t) = \chi_{A2}\,\psi_{A2}(r) \exp[i(qz - \omega t + n\phi)]/k_{A,2}, \quad (6c)$$

where

$$\psi_{A0}(r) = I_n(\kappa_{A,0}\,r)\;\theta\,(q\,v_{A,0} - \omega) + J_n(k_{A,0}\,r)\;\theta\,(\omega - q\,v_{A,0}), \quad (7a)$$

$$\psi_{Aj}(r) = J_n(k_{A,j}\,r), \quad (7b)$$

for $j = 1$ and 2. Here, $I_n(x)$ and $J_n(x)$ are the first kind of modified Bessel function and Bessel function of the order n, respectively. $\kappa_{A,0}$ and $k_{A,j}$ ($j = 0$, 1, and 2) are the lateral wave vectors defined by

$$\kappa_{A,0} = \sqrt{q^2 - \left(\frac{\omega}{v_{A,\mathrm{LA}}}\right)^2}, \quad (8a)$$

$$k_{A,0} = \sqrt{\left(\frac{\omega}{v_{A,\mathrm{LA}}}\right)^2 - q^2}, \quad (8b)$$

$$k_{A,1} = k_{A,2} = \sqrt{\left(\frac{\omega}{v_{A,\mathrm{TA}}}\right)^2 - q^2}. \quad (8c)$$

For the surrounding medium, the potential functions are given by

$$\phi_{B0}(\mathbf{r},t) = [\chi_{B01}\,\psi_{B01}(r) + \chi_{B02}\,\psi_{B02}(r)] \exp[i(qz - \omega t + n\phi)], \quad (9a)$$

$$\phi_{B1}(\mathbf{r},t) = [\chi_{B11}\,\psi_{B11}(r) + \chi_{B12}\,\psi_{B12}(r)] \exp[i(qz - \omega t + n\phi)], \quad (9b)$$

$$\phi_{B2}(\mathbf{r},t) = [\chi_{B21}\,\psi_{B21}(r) + \chi_{B22}\,\psi_{B22}(r)] \exp[i(qz - \omega t + n\phi)]/k_{B,2}, \quad (9c)$$

where

$$\psi_{B01(2)}(r) = I_n(\kappa_{B,0}\,r)\,[K_n(\kappa_{B,0}\,r)]\;\theta\,(q\,v_{B,0} - \omega) + J_n(k_{B,0}\,r)\,[Y_n(k_{B,0}\,r)]\,\theta\,(\omega - q\,v_{B,0}), \quad (10a)$$

$$\psi_{Bj1(2)}(r) = J_n(k_{B,j}\,r)\,[Y_n(k_{B,j}\,r)], \quad (10b)$$

for $j = 1$ and 2. $K_n(x)$ and $Y_n(x)$ are the second kind of modified Bessel function and Bessel function of the order n. The lateral wave vectors $\kappa_{B,0}$ and $k_{B,j}$ ($j = 0$, 1, and 2) yield

$$\kappa_{B,0} = \sqrt{q^2 - \left(\frac{\omega}{v_{B,\mathrm{LA}}}\right)^2}, \quad (11a)$$

$$k_{B,0} = \sqrt{\left(\frac{\omega}{v_{B,\mathrm{LA}}}\right)^2 - q^2}, \quad (11b)$$

$$k_{B,1} = k_{B,2} = \sqrt{\left(\frac{\omega}{v_{B,\mathrm{TA}}}\right)^2 - q^2}. \quad (11c)$$

The stress field is explicitly given by using the displacement vector.[31] The coefficients $\chi_{\alpha i}$ are determined for each rotational symmetry order n by applying the boundary conditions of continuity of displacement vector and stress fields at the wire-surrounding interface.

III. EXTENDED PHONON MODES

Extended acoustic-phonon modes are characterized by the rotational symmetry order n. For $n = 0$, the coefficients $\chi_{\alpha 0}$ and $\chi_{\alpha 2}$ decouple from $\chi_{\alpha 1}$ because the matrix elements joining $\chi_{\alpha 1}$ to $\chi_{\alpha 0}$ and $\chi_{\alpha 2}$ vanish. As a result, there are two kinds of azimuthally symmetric phonon modes. The mode due to $\nabla \times \mathbf{\Psi_1}$ is referred to as a torsional mode and the other due to the sum of the terms $\nabla\phi_0 + \nabla \times \nabla \times \mathbf{\Psi}_2$ is referred to as a dilatational mode, according to the particle motion in a solid. For a finite integer n, there is no longer decoupling among the coefficients. All the waves are coupled into phonon modes termed flexural modes, whose displacement vector is expressed by Eq. (1). In the following subsections, we investigate each phonon mode and its resonant modes.

A. Torsional mode

The displacement vector of the torsional mode has only the azimuthal component u_ϕ. Figure 2(a) shows the amplitude w_ϕ, defined by $u_\phi = w_\phi \exp[i(qz - \omega t)]$, versus distance r in the radial direction at frequencies $\nu = 0.70$ and 0.78 THz for $R = 100$ Å. Here, the reduced longitudinal wave number qR is set to $qR = 6$. The envelope of amplitudes decreases as $r^{-1/2}$ in the surrounding medium for both cases, and there is no difference between the cases except for the variation in the wire. The amplitude at $\nu = 0.78$ THz in the wire is obviously reduced from that at $\nu = 0.70$ THz. To see the difference more clearly, we plot the squared absolute displacement multiplied by r, $r|u_\phi|^2$, for both the cases in Fig. 2(b). The envelopes of the mode at $\nu = 0.70$ THz in the wire and surrounding medium are connected smoothly at the wire-surrounding interface. In contrast to this case, a discontinuity of the envelope develops at the interface in the case of $\nu = 0.78$ THz. The magnitude of $r|u_\phi|^2$ in the wire becomes approximately 0.7 times as large as that in the surrounding medium.

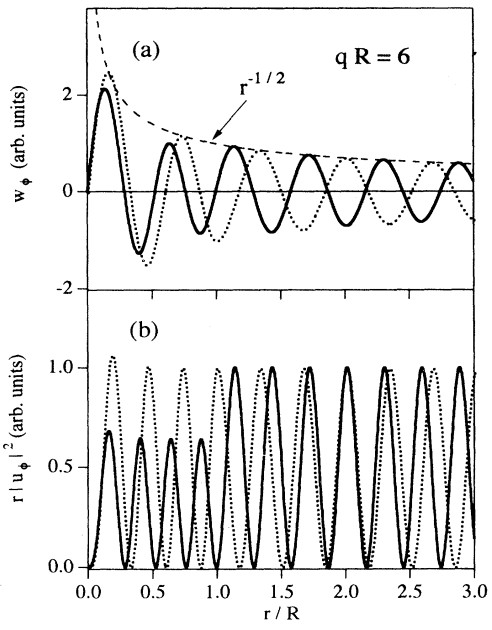

FIG. 2. (a) Amplitudes w_ϕ of the torsional acoustic-phonon mode versus distance r in the radial direction. The dotted and solid lines denote the amplitude at $\nu = 0.70$ and 0.78 THz for $R = 100$ Å, respectively. The dashed line is the envelope function $r^{-1/2}$. The reduced longitudinal wave vector qR is fixed at 6. (b) The squared absolute displacement multiplied by r, $r|u_\phi|^2$, versus r. The reduction of amplitude for $\nu = 0.78$ THz in the wire is apparent.

For quantitative comparison, we introduce the ratio F of averaged $r|\mathbf{u}|^2$ in the wire to that in the whole system defined by

$$F = \frac{1}{R}\int_0^R r|\mathbf{u}|^2 dr \Big/ \lim_{R_s\to\infty} \frac{1}{R_s}\int_0^{R_s} r|\mathbf{u}|^2 dr. \qquad (12)$$

In Eq. (12), we assume the surrounding medium to be a cylinder with radius R_s, which is taken to be infinite after integration. The ratio F gives the ratio of the squared envelope of the amplitude in the wire to that in the surrounding medium at the wire-surrounding interface. F should be unity unless we take into account the effects of the Q1D wire structures on phonon modes. Therefore the phonon modes, when $F > 1$, are concentrated in the wire region in comparison with those of the plain bulk systems without the Q1D wire structures. On the other hand, the phonon modes are suppressed in the wire for $F < 1$. In contrast to these cases, the phonon modes for $F = 1$ are entirely extended in both the wire and surrounding medium like bulk phonon modes in the plain bulk systems.

The F of the torsional extended phonon mode versus frequency is plotted for $R = 100$ Å in Fig. 3, for several

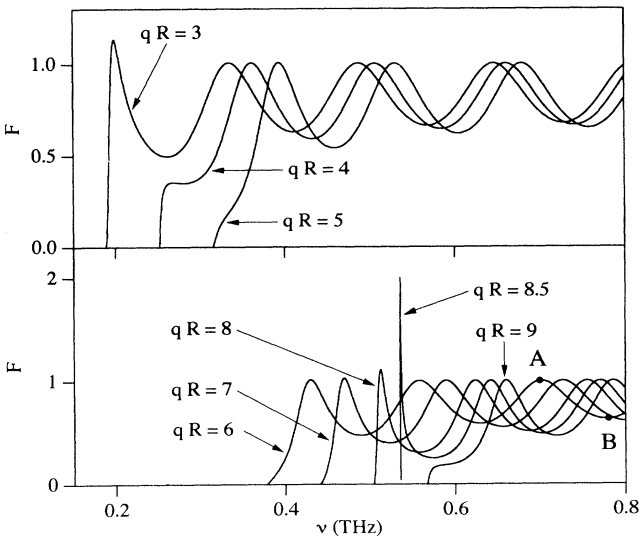

FIG. 3. Ratio F of the torsional phonon mode versus frequency for $R = 100$ Å. Peaks and valleys appear periodically for various magnitudes of the reduced longitudinal wave vector qR, and the peak heights are almost unity, except for the peaks for $qR = 8.5$.

magnitudes of the reduced longitudinal wave number qR in the frequency region $\omega \geq q\,v_{\mathrm{AlAs,TA}}$. F is not a monotonic function of frequency but has peaks and valleys, which appear alternately and shift to the high-frequency region with the increase in qR. The peak heights are unity, independent of frequency and of the reduced longitudinal wave number qR, except for a few peaks. Sharpening of peaks and substantial increases of their heights are found in the vicinity of the bulk-$\mathrm{TA_{AlAs}}$ dispersion, and the spiky peaks disappear with an increase of qR, e.g., from $qR = 8.5$ to 9.0. On the other hand, the valleys become deeper, nearing the bulk-$\mathrm{TA_{AlAs}}$ dispersion and the valleys near the bulk-$\mathrm{TA_{AlAs}}$ dispersion disappear with the increase in qR.

The variation of F reflects resonance of phonons in the Q1D wires. Then we hereafter refer to the phonon modes at the peaks with $F \geq 1$ as resonant modes and term, for convenience, the trajectories of the peak positions in the ω-q plane the dispersions of the resonant phonon modes.

As denoted in Fig. 3, the cases for $\nu = 0.70$ THz and $\nu = 0.78$ THz correspond to a peak (A) and valley (B), respectively. The amplitude at the wire surface at $\nu = 0.70$ THz has a local maximum, ignoring its sign, and the amplitude at $\nu = 0.78$ THz becomes a node. Then we may compare the peaks to the phonon modes of a free-standing wire and the valleys to those of a wire with a fixed boundary. Figure 4 illustrates the dispersion relations of resonant modes together with those of phonon modes in a free-standing wire for $R = 100$ Å. The thick solid lines and the open circles denote the dispersions of the resonant torsional modes and torsional phonon mode of a free-standing wire with the same radius, respectively. The dispersions of the resonant modes almost coincide with those of the torsional phonon mode of a free-standing wire.

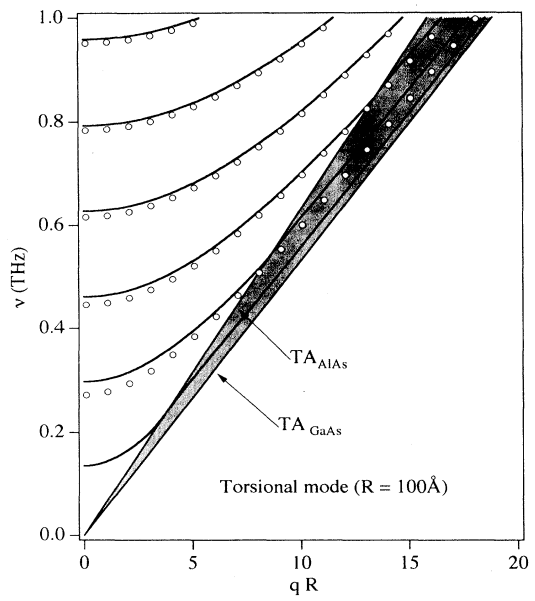

FIG. 4. Dispersions of the resonant torsional modes for $R = 100$ Å. The thick solid lines denote the dispersions and the thin lines in the shaded region between the bulk-$\mathrm{TA_{GaAs}}$ and -$\mathrm{TA_{AlAs}}$ dispersion curves are those of the confined torsional phonon mode (Ref. 31). The open circles denote the dispersions of the torsional phonon mode of a free-standing wire with the same radius.

In the shaded frequency region $\omega < q\,v_{\mathrm{AlAs,TA}}$ in Fig. 4, acoustic phonons are confined to the quantum wire and the dispersions of the confined phonon modes have subband structures.[31] F diverges for the confined modes. Then the sharpening of the peaks for the extended phonon modes near the bulk-$\mathrm{TA_{AlAs}}$ dispersion curve may be related to transition of the extended phonon modes to confined ones. The thin solid lines in the shaded region of Fig. 4 denote the dispersions of the confined torsional mode. The dispersions of the resonant modes are linked to those of the confined torsional mode at the bulk-$\mathrm{TA_{AlAs}}$ dispersion curve as we expected. Then we can attribute the substantial increase of amplitude in the wire to the transition of extended phonon modes to confined phonon modes.

B. Dilatational mode

The dilatational phonon mode is the other azimuthal symmetric phonon mode, whose displacement vector $\mathbf{u}$ has only the radial u_r and axial components u_z in contrast to the torsional mode. Defining the amplitude $\mathbf{w}$ of the displacement vector field by $\mathbf{u} = \mathbf{w}\exp[i(qz - \omega t)]$, the phase of the axial component w_z of the amplitude is shifted by $\pi/2$ from the radial component w_r. Figure 5(a) illustrates the amplitudes of the dilatational mode versus r at $\nu = 0.50$ THz, where $qR = 7$, and Fig. 5(b) plots $r|\mathbf{u}|^2$ versus r. A large reduction of $r|\mathbf{u}|^2$ in the wire is found in comparison with that in the surrounding medium.

Figure 6 shows the F of the dilatational mode versus frequency for some reduced longitudinal wave numbers qR in the frequency region $q\,v_{\mathrm{AlAs,TA}} < \omega < q\,v_{\mathrm{AlAs,LA}}$. There are two kinds of peaks in this frequency region: one is the small peaks which appear in the lower frequency side of the region, and the other is the large peaks which appear in the higher frequency side. The small peaks are broad and their heights are approximately unity. However, the small peaks become spiky and larger as they near the bulk-$\mathrm{TA_{AlAs}}$ dispersion. These features of the small peaks suggest that the resonant dilatational phonon modes are the same kind of resonant torsional modes and are related to the confined dilatational phonon mode.

In contrast to the small peaks, the large peaks are always spiky, independent of the bulk-$\mathrm{TA_{AlAs}}$ dispersion, and are an order of magnitude larger than the small peaks, which means extremely large amplitude in the wire. The large peaks do not disappear, and the number of the spiky peaks increases with the reduced longitudinal wave number qR. Thence the spiky peaks imply another kind of resonant phonon mode.

To make the difference clear between the resonant dilatational phonon modes with the small F (≈ 1) and large F ($\gg 1$), we examine the contribution of the

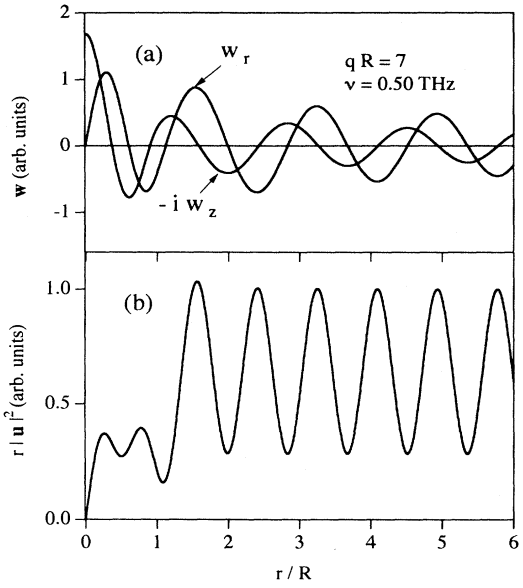

FIG. 5. (a) The radial w_r and axial w_z components of displacement of the dilatational phonon modes at $\nu = 0.50$ THz for $R = 100$ Å and (b) the corresponding $r|\mathbf{u}|^2$ versus r in the radial direction. The reduced longitudinal wave number is set at $qR = 7$. The phase factor of radial and axial components of the displacement are shifted by $\pi/2$. The amplitude in the wire is found to be extremely reduced in comparison with that in the surrounding medium.

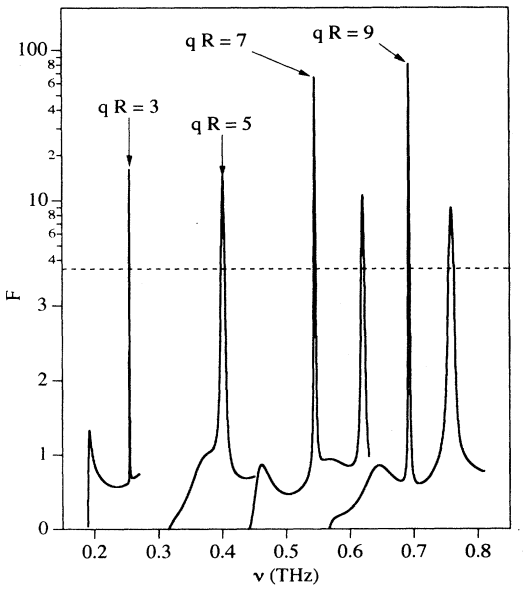

FIG. 6. Ratio F of the dilatational phonon mode versus frequency for $R = 100$ Å in the frequency region $q v_{\mathrm{AlAs,TA}} < \omega < q v_{\mathrm{AlAs,LA}}$, for several magnitudes of the reduced longitudinal wave number qR. Small and large peaks are found. The dashed horizontal line denotes the change of scale from a linear to a logarithmic one.

LA wave to the dilatational mode in the wire. Figure 7(a) shows the relative contribution of the LA wave, $\chi_{A0}{}^2/(\chi_{A0}{}^2 + \chi_{A2}{}^2)$, to the dilatational phonon mode versus frequency at $qR = 7$, and Fig. 7(b) plots the corresponding F of the dilatational mode versus frequency. The arrow in Fig. 7 denotes the frequency $\nu_{\mathrm{GaAs,LA}}$ (= 0.524 THz) of the bulk-$\mathrm{LA_{GaAs}}$ phonon mode at $qR = 7$. The LA wave in the wire changes from an evanescent wave to a real one at the frequency $\nu_{\mathrm{GaAs,LA}}$. Below the frequency, the contribution of the LA wave to the dilatational mode is negligible. The dilatational mode is mainly attributed to the TA wave and the displacement vector can be approximately expressed as $\mathbf{u} \approx \nabla \times \nabla \times \mathbf{\Psi}_2$ in this frequency region. Consequently, the dilatational mode effectively becomes the shear wave mode perpendicular to the torsional mode. These results demonstrate that, although the relevant phonon mode is referred to as the dilatational mode, the dilatational mode does not induce local volume change below $\nu_{\mathrm{GaAs,LA}}$. Hence the resonant dilatational modes with small F, which appear in this frequency region, are effectively shear wave modes.

Above $\nu_{\mathrm{GaAs,LA}}$, there are two peaks in the relative contribution of the LA wave to the dilatational mode. The peak heights are approximately unity, and the rates stay low at about 0.1 between the peaks. The behavior of the rates obviously correlates to the F. Then the resonant dilatational modes with large F are solely attributed to the LA wave component. In the frequency region between the resonant dilatational modes, the dilatational mode is mostly attributed to the TA wave. The volume change due to the dilatational mode is roughly propor-

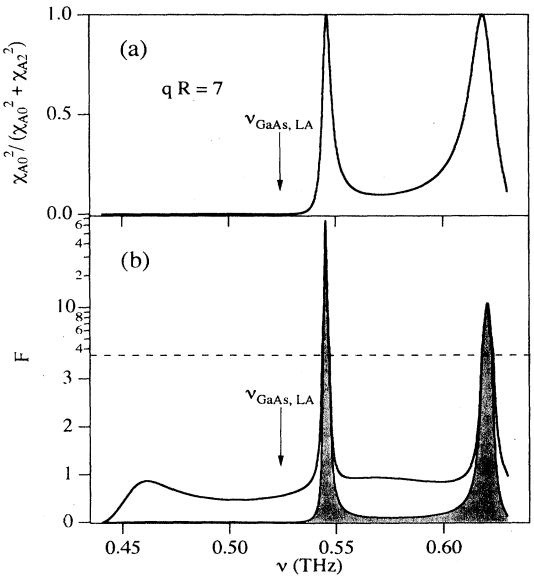

FIG. 7. (a) Contribution of the LA wave to the dilatational phonon mode versus frequency and (b) the corresponding F for $R = 100$ Å. The reduced longitudinal wave number is set at $qR = 7$. The shaded region in (b) denotes the F solely attributed to the LA wave in the wire. The dashed horizontal line in (b) denotes the change of scale from a linear to a logarithmic one.

tional to the square root of the product of ratio F and the relative contribution of the LA wave to the dilatational mode. The volume change in the wire, as a result, takes place only around the resonant dilatational modes with large F and is suppressed in the frequency region between the resonant modes. The shaded region in Fig. 7(b) denotes F, omitting the contribution of the TA wave in the wire to the F, which confirms that the volume change is induced at around the resonant dilatational modes with large F.

Owing to the different features of the two kinds of resonant dilatational modes, we expect two kinds of dispersions of these modes. Figure 8 shows the dispersions of the resonant dilatational modes together with the dispersions of the confined dilatational mode. The thin and thick solid lines denote the dispersions of the resonant dilatational modes with small F and large F, respectively. The dispersions of the resonant dilatational modes with small F have subband structures, which begin at the bulk-LA_{GaAs} dispersion curve and are linked to those of the confined phonon modes denoted by the dashed lines, at the bulk-TA_{AlAs} dispersion curve. In contrast to this case, the dispersions of the resonant modes with large F begin at the bulk-LA_{AlAs} dispersion curve and tend to the bulk-LA_{GaAs} dispersion curve with the increase in the reduced longitudinal wave number qR. However, they do not intersect the bulk-LA_{GaAs} dispersion curve, and exhibit subband structures similar to those of the confined phonon modes. Based on these features concerning the displacements and the dispersions, we may conclude that the resonant modes with large F are quasiconfined phonon modes with dilatation.

In the frequency region $\omega > q v_{AlAs,LA}$, the LA waves become real waves in both the wire and surrounding medium. Then, the six waves are connected at the wire-surrounding interface so that they satisfy the boundary conditions. Since four boundary conditions are applied on the displacement and stress fields, two coefficients can be taken arbitrarily. For example, any combinations of arbitrary χ_{A0} and χ_{A2} are permitted. Then, we examine the extended phonon modes in the following two cases: (1) when the displacement in the wire is solely attributed to an LA wave and (2) when it is attributed to a TA wave.

Figure 9 shows the ratio F versus frequency for both the cases, where $q = 0$. The solid and dashed lines denote the polarization of the phonon mode: the longitudinal (L) and transverse (T) wave in the wire, respectively. The ratio F oscillates with frequency as in the case of the torsional mode (Fig. 3), and the peak heights are approximately unity, irrespective of the polarization of the mode in the wire. We observe the same kind of oscillation of the F for finite longitudinal wave numbers qR. Then, in this frequency region, only entirely extended resonant modes exist. The dispersions of the resonant modes are plotted in Fig. 8 by the solid (L) and dashed (T) lines, tending toward the bulk-LA_{AlAs} dispersion curve with increasing qR. However, the dispersion curves disappear on the way since the magnitude of ratio F becomes smaller than unity as it nears the LA_{AlAs} dispersion curve.

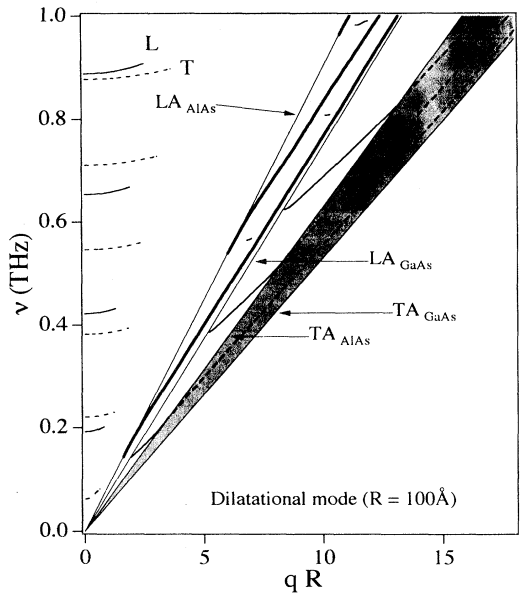

FIG. 8. Dispersions of the resonant dilatational phonon modes for $R = 100$ Å. The thick and thin solid lines in the frequency region $q v_{AlAs,TA} < \omega < q v_{AlAs,LA}$ denote the quasiconfined and entirely extended resonant modes, respectively. The dashed lines in the shaded region between the bulk-TA_{GaAs} and TA_{AlAs} dispersion curves are the dispersions of the confined dilatational modes (Ref. 31). The solid (L) and dashed (T) lines in the region $\omega > q v_{AlAs,LA}$ are the dispersions of the entirely extended resonant modes attributed solely to the LA wave and TA wave in the wire, respectively.

C. Flexural modes

Since the degrees of freedom exceed the number of the boundary conditions by two in the frequency region

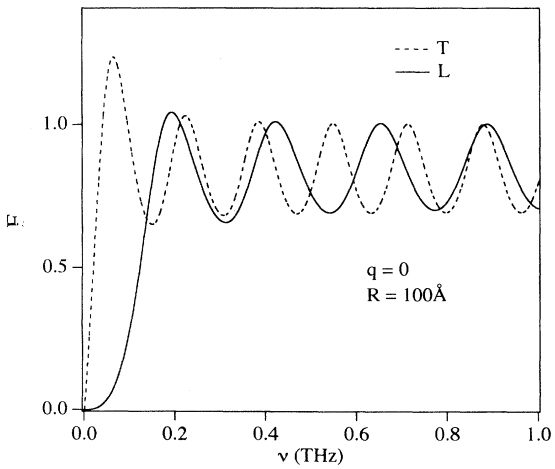

FIG. 9. Ratio F of the dilatational phonon modes versus frequency for $R = 100$ Å in the region $\omega > q v_{AlAs,LA}$. The solid and dashed lines in the region $\omega > q v_{AlAs,LA}$ are the dispersions of the resonant modes solely due to the LA wave and TA wave in the wire, respectively. The longitudinal wave number is taken as $q = 0$.

$q v_{\mathrm{AlAs,TA}} < \omega < q v_{\mathrm{AlAs,LA}}$, two of eight coefficients can be taken to be arbitrary. Then we investigate the flexural modes in the cases $[A]$ ($\chi_{A0} = 1, \chi_{A1} = 0$), $[B]$ ($\chi_{A0} = 1, \chi_{A2} = 0$), and $[C]$ ($\chi_{A0} = 0, \chi_{A1} = 1$).

Figure 10(a) illustrates the amplitudes of the flexural mode with $n = 1$ and Fig. 10(b) the corresponding $r|\mathbf{u}|^2$ for case $[A]$. The azimuthal w_ϕ and axial amplitude components w_z differ in phase from the radial component w_r by $\pi/2$. The azimuthal component w_ϕ vanishes and the radial w_r and axial components w_z coincide at the wire axis due to the rotational symmetry of the mode.[31] The amplitudes are very large in the wire as compared with those of the surrounding medium. Such large amplitudes are observed for the quasiconfined phonon modes.

Figure 11(a) illustrates the ratio F versus frequency for the three cases in the frequency region $q v_{\mathrm{AlAs,TA}} < \omega < q v_{\mathrm{AlAs,LA}}$ for $qR = 8$ and Fig. 11(b) shows the corresponding relative contribution of the LA wave to the flexural mode with $n = 1$. F has small and large peaks like the dilatational mode, denoting the entirely extended and quasiconfined resonant phonon modes. Aside from the small peaks whose height is lower than unity, there are two small peaks at $\nu = 0.56$ and 0.68 THz in case $[C]$, which coincide with the small peaks of case $[B]$. The large peak at ν=0.65 THz exists in cases $[A]$ and $[B]$. Thus case $[B]$ has mixed spectra of cases $[A]$ and $[C]$. The relative contributions of the LA wave to the flexural mode also correlate to ratio F, which confirms that the local volume change is induced at around the quasiconfined phonon modes and that the entirely extended resonant modes are effectively the shear wave modes. The amplitude in the wire or ratio F of the quasiconfined phonon modes decreases with mixing of the TA wave component, and the quasiconfined modes disappear in case $[C]$, where there is no contribution of the LA wave to the flexural mode. The facts confirm that the LA wave is essential to the quasiconfined phonon modes.

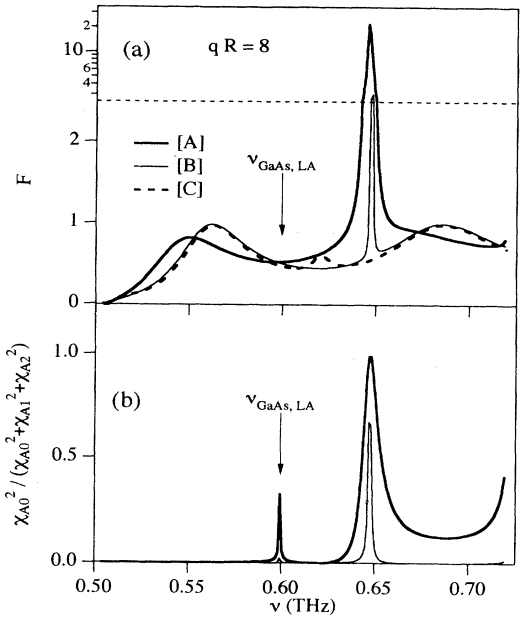

FIG. 11. (a) Ratio F of the flexural phonon mode with $n = 1$ versus frequency for $R = 100$ Å in the frequency region $q v_{\mathrm{AlAs,TA}} < \omega < q v_{\mathrm{AlAs,LA}}$ and (b) the corresponding contribution of the LA wave to the flexural phonon at $qR = 8$. The thick solid, thin solid, and dashed lines correspond to cases $[A]$, $[B]$, and $[C]$ discussed in the text, respectively. The dashed horizontal line in (a) denotes the change of scale from a linear to a logarithmic one.

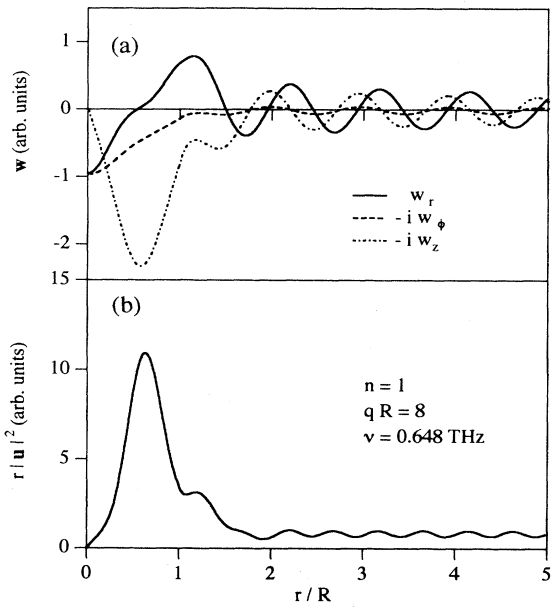

FIG. 10. (a) The radial, axial, and azimuthal components of amplitude $\mathbf{w}$ of the flexural phonon mode with $n = 1$ at $\nu = 0.648$ THz and $qR = 8$ for $R = 100$ Å and (b) the corresponding $r|\mathbf{u}|^2$ versus r in the radial direction. The amplitude in the wire is found to be extremely enlarged in comparison with that in the surrounding medium.

Figure 12 shows the dispersions of the resonant flexural modes of case $[B]$ with $n = 1$ together with the dispersions of the confined flexural mode with $n = 1$. Here, we note that the mixture of dispersions of cases $[A]$ and $[C]$ coincides with the dispersions of case $[B]$ as mentioned above. Then we may regard the dispersions of case $[B]$ as those for the arbitrary combinations of coefficients. The thin and thick solid lines denote the entirely extended and quasiconfined resonant modes, respectively. These resonant modes have subband structures of dispersions similar to those of the dilatational mode, except that the dispersions of both resonant modes start at the bulk-$\mathrm{LA_{AlAs}}$ dispersion curve.

In the frequency region $\omega > q v_{\mathrm{AlAs,LA}}$, since the LA wave in the surrounding medium becomes a real wave, the degrees of freedom exceed the number of boundary conditions by three. As a result, three of the nine coefficients, e.g., χ_{A0}, χ_{A1}, and χ_{A2}, are taken to be arbitrary. Then we examine the flexural modes in the three cases: $[I]$ ($\chi_{A0} = 1, \chi_{A1} = 0, \chi_{A2} = 0$), $[II]$ ($\chi_{A0} = 0$, $\chi_{A1} = 1$, $\chi_{A2} = 0$), and $[III]$ ($\chi_{A0} = 0, \chi_{A1} = 0, \chi_{A2} = 1$).

Figure 13 shows the ratio F versus frequency for the

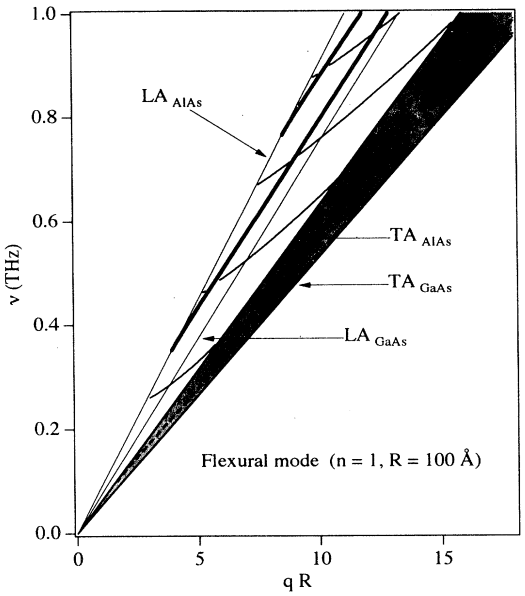

FIG. 12. Dispersions of the resonant flexural phonon modes in the frequency region $q v_{\mathrm{AlAs,TA}} < \omega < q v_{\mathrm{AlAs,LA}}$ for $R = 100$ Å. The thick and thin solid lines denote the dispersions of the quasiconfined and entirely extended resonant phonon modes, respectively. The dashed lines in the shaded region $q v_{\mathrm{GaAs,TA}} < \omega < q v_{\mathrm{AlAs,TA}}$ are the dispersions of the confined flexural phonon mode with $n = 1$.

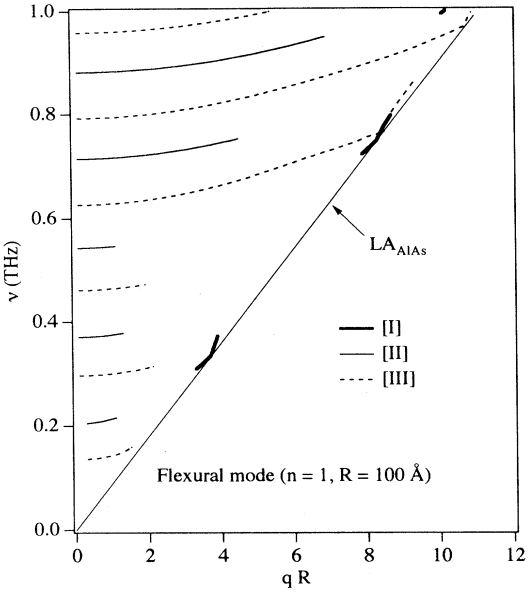

FIG. 14. Dispersions of the resonant flexural phonon modes with $n = 1$ in the frequency region $\omega > q v_{\mathrm{AlAs,LA}}$ for $R = 100$ Å. The thick solid, thin solid, and dashed lines denote the same cases $[I]$, $[II]$, and $[III]$ as Fig. 13.

three cases, where $q = 0$. Ratio F varies oscillationally with frequency for all the cases. The peak heights depend on the cases and are an order of unity. Such oscillations of ratio F are found for finite longitudinal wave numbers qR and the peak heights of ratio F decrease as they near the bulk $\mathrm{LA_{AlAs}}$ dispersion curve. Figure 14 illustrates the dispersions of the three cases, confirming the disappearance of the dispersions on the way to the bulk-$\mathrm{LA_{AlAs}}$ dispersion curve for cases $[II]$ and $[III]$. The F of case $[I]$ is almost lower than unity in this frequency region; however, the ratio exceeds unity in the vicinity of the bulk-$\mathrm{LA_{AlAs}}$ dispersion curve, where the dispersions of the quasiconfined modes terminate. Thence the appearance of case $[I]$ near the dispersion curve of the bulk-$\mathrm{LA_{AlAs}}$ waves is due to the transition to the quasiconfined modes as seen for the resonant torsional modes.

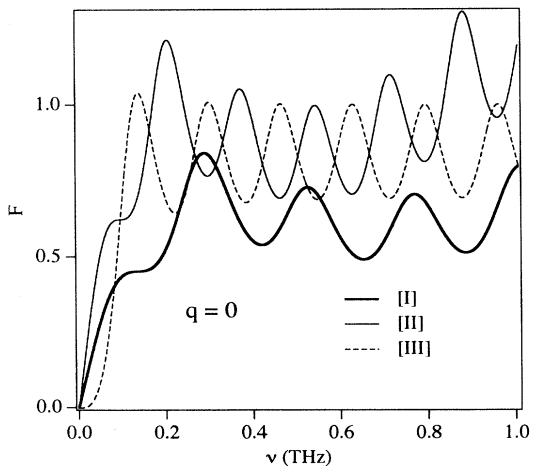

FIG. 13. Ratio F of the flexural phonon modes versus frequency for $R = 100$ Å in the region $\omega > q v_{\mathrm{AlAs,LA}}$. The thick solid, thin solid, and dashed lines correspond to cases $[I]$, $[II]$, and $[III]$ discussed in the text, respectively. The longitudinal wave number is taken as $q = 0$.

As for the flexural modes with $n \geq 2$, there are the same two kinds of resonant modes as with $n = 1$. However, the dispersions of the resonant flexural modes shift to the high-frequency region with increasing n. The flexural mode with a negative rotational symmetry order $-n$ is the same as that with a positive order n, except for the sign of the azimuthal component of displacements. Then we have the same two kinds of resonant modes for both cases.

D. Density of states

Finally we investigate the density of states (DOS) of extended acoustic-phonon modes. Here, we consider a huge free-standing cylinder of AlAs with radius R_s and length L ($L \gg R_s$), surrounding a quantum wire. Spectra of phonon modes are determined by the boundary conditions on the cylinder surface, ignoring the effects of cylinder ends. Modifications in the spectra due to the quantum wire will be negligible. Hence we may examine the DOS of the extended phonon modes based on spectra of phonons in a huge free-standing cylinder of AlAs

without a quantum wire.

The dispersion relation of the torsional mode yields from Eq. (8c),

$$\omega = v_{\mathrm{TA}}\sqrt{q^2+k^2}, \tag{13}$$

since the torsional mode is solely attributed to a TA wave. The longitudinal and lateral wave numbers, q and k, are quantized, and then there is one allowed value of (k,q) per volume $2\pi^2/L\,R_s$ in (k,q) space. The DOS, $D_t(\omega)$, of the torsional mode is readily obtained as

$$D_t(\omega) = \frac{L\,R_s}{2\pi}\,\frac{\omega}{{v_{\mathrm{TA}}}^2}. \tag{14}$$

In contrast to the torsional mode, it is hard to express analytically the dispersion relations of the dilatational and flexural modes, because these modes are coupled modes of LA and TA waves. Then we introduce a phase velocity v for these modes, which is determined below, and assume that the LA and TA waves have the same phase velocity v. Considering a cylindrical wave, whose potential functions ϕ_i are given by

$$\phi_i(\mathbf{r}) = \frac{\chi_i}{\sqrt{r}}\,e^{i(kr+n\theta+qz-\omega t)}, \tag{15}$$

and substituting Eq. (15) into (4), we obtain the following dispersion relation for the dilatational and flexural modes,

$$\omega = v\sqrt{q^2+k^2+\frac{n^2}{{R_s}^2}}, \tag{16}$$

which is qualitatively in good agreement with the numerically obtained data.[30] Equation (16) shows that there is a finite lowest frequency ω_n^0 $(=v\,n/R_s)$ for a flexural mode with rotational symmetry order n. The DOS of the dilatational and flexural modes yields

$$D_n(\omega) = \frac{L\,R_s}{2\pi}\,\frac{\omega}{v^2}\,\theta(\omega-\omega_n^0). \tag{17}$$

The DOS of the dilatational and flexural modes is almost the same as that of the torsional mode (14), but changes discontinuously from zero to $L\,R_s\,\omega_n^0/2\pi v^2$ at ω_n^0, due to the step function in Eq. (17). The jump in the DOS is attributed to the van Hove singularity at $q=k=0$, where the group velocity becomes zero.

The frequency dependence of each phonon mode is different from that of the bulk phonons in the Debye approximation. This is because the rotational symmetry order of phonon modes is fixed. Therefore, the ω^2 dependence of the DOS for 3D bulk phonon systems is recovered by summing the DOS of all the phonon modes. The total DOS, $D(\omega)$, is given by

$$D(\omega) = D_t(\omega) + \sum_{n=-\infty}^{\infty} D_{|n|}(\omega). \tag{18}$$

Substituting Eqs. (14) and (17) into (18), the $D(\omega)$ yields

$$\begin{aligned} D(\omega) &= \frac{L\,R_s}{2\pi}\left(\frac{1}{{v_{\mathrm{TA}}}^2}+\frac{1}{v^2}\right)\omega + \frac{L\,{R_s}^2}{\pi}\,\frac{\omega^2}{v^3} \\ &\simeq \frac{L\,\pi\,{R_s}^2\,\omega^2}{\pi^2\,v^3} = \frac{V\,\omega^2}{\pi^2\,v^3}, \end{aligned} \tag{19}$$

for a large R_s, where V denotes the volume of the system. The total DOS should coincide with the DOS of the 3D Debye model given by

$$D_D(\omega) = \frac{3\,V\,\omega^2}{2\pi^2}\left\langle\frac{1}{v^3}\right\rangle, \tag{20}$$

where

$$\left\langle\frac{1}{v^3}\right\rangle = \frac{1}{3}\left(\frac{1}{{v_{\mathrm{LA}}}^3}+\frac{2}{{v_{\mathrm{TA}}}^3}\right). \tag{21}$$

Comparing them, the phase velocity v of the dilatational and flexural modes is given, in terms of LA and TA wave velocities, by

$$\frac{1}{v^3} = \frac{1}{2}\left(\frac{1}{{v_{\mathrm{LA}}}^3}+\frac{2}{{v_{\mathrm{TA}}}^3}\right). \tag{22}$$

We note here that, although the total DOS is useful for studies on thermal properties of the system, it is less important for electron-phonon scattering. Because of the full axial symmetry of the system, the total angular momentum of electrons and phonons about the wire axis has to be conserved for electron scattering via the deformation potential,[32] defining the angular momentum of phonons with rotational symmetry order n to be $\hbar n$. This means that only the phonons with certain rotational symmetry contribute to electron scattering. Therefore, the DOS of each phonon mode, D_t and D_n, has significance for electron scattering instead of the total DOS.

IV. SUMMARY AND DISCUSSION

In this paper, we analytically investigated the resonant acoustic-phonon modes in a cylindrical GaAs quantum wire within bulk AlAs, paying special attention to the displacement in the wire region. The extended acoustic-phonon modes are the coupled modes of the LA and TA waves, classified into torsional, dilatational, and flexural phonon modes according to the rotational symmetry of the modes. The displacement in the wire region is suppressed or enhanced in comparison with that assuming the plain bulk systems without Q1D wires. The enhancement of displacement in the wire region is attributed to the resonant modes related to the wire dimensions. There are two kinds of resonant modes: one is the quasiconfined phonon modes and the other is entirely extended phonon modes. The quasiconfined phonon modes have substantially large displacement in the wire region, in contrast to the entirely extended phonon modes. These resonant modes have dispersion relations with subband structures similarly to the confined phonon modes in a free-standing wire. These results lead to the conclusion that, in the wire region, the extended phonon modes have

characters of confined phonon modes in a free-standing wire rather than the usual bulk phonon modes, although a 3D bulk character was assumed for acoustic phonons in most studies of electron scattering.

We have shown that the amplitude in the wire of the extended acoustic-phonon modes is substantially modulated, depending on frequency and the longitudinal wave vector. Considering the electron-phonon interaction, the large/small amplitude in the wire will result in enhancement/reduction of the coupling, regardless of the type of interaction. In addition to the modifications in amplitudes in a wire, the DOS of phonons associated with electron scattering has different frequency dependence from that of the usual 3D bulk phonons. Thence the phonon modes peculiar to the Q1D wire systems, including the confined phonon modes,[31] are expected to cause further modifications in electron transport phenomena.

ACKNOWLEDGMENTS

The author would like to thank K. Barrymore for useful comments on the manuscript. This work is supported in part by a Grant-in-Aid for Scientific Research from the Ministry of Education, Science, and Culture of Japan (Grant No. 05650048).

[1] J. Cibert, P. M. Petroff, G. J. Dolan, S. J. Pearton, A. C. Gossard, and J. H. Englishman, Appl. Phys. Lett. **49**, 1275 (1986).
[2] J. Seyler and M. N. Wybourne, Phys. Rev. Lett. **69**, 1427 (1992).
[3] C. Lettau, M. Wendel, A. Schmeller, W. Hansen, and J. P. Kotthaus, Phys. Rev. B **50**, 2432 (1994).
[4] V. K. Arora, Phys. Rev. B **23**, 5611 (1981).
[5] G. Fishman, Phys. Rev. B **34**, 2394 (1986).
[6] G. Fishman, Phys. Rev. B **36**, 7448 (1987).
[7] M. A. Stroscio, Phys. Rev. B **40**, 6428 (1989).
[8] U. Bockelmann and G. Bastard, Phys. Rev. B **42**, 8947 (1990).
[9] P. P. Basu, D. Chattopadhyay, and P. C. Rakshit, Phys. Rev. B **46**, 13 254 (1992).
[10] V. B. Campos and S. Das Sarma, Phys. Rev. B **46**, 3849 (1992).
[11] W.S. Li, S. W. Gu, T. C. Au-Yeung, and Y. Y. Yeung, Phys. Lett. A **166**, 377 (1992).
[12] J. R. Senna and S. Das Sarma, Phys. Rev. Lett. **70**, 2593 (1993).
[13] S. Das Sarma and V. B. Campos, Phys. Rev. B **47**, 3728 (1993).
[14] N. Telang and S. Bandyopadhyay, Appl. Phys. Lett. **62**, 3161 (1993).
[15] B. Tanatar, J. Phys. Condens. Matter **5**, 2203 (1993).
[16] F. Comas, C. Trallero-Giner, and A. Cantarero, Phys. Rev. B **47**, 7602 (1993).
[17] S. Das Sarma and V. B. Campos, Phys. Rev. B **49**, 1867 (1994).
[18] Y. Tokura and S. Tarucha, Phys. Rev. B **50**, 10 981 (1994).
[19] H. Sakaki, Jpn. J. Appl. Phys. **19**, L735 (1980).
[20] A. K. Sood, J. Menéndez, M. Cardona, and K. Ploog, Phys. Rev. Lett. **54**, 2111 (1985).
[21] G. Fasol, M. Tanaka, H. Sakaki, and Y. Horikoshi, Phys. Rev. B **38**, 6056 (1988).
[22] M. Watt, C. M. Sotomayor-Torres, H. E. G. Arnot, and S. P. Beaumont, Semicond. Sci. Technol. **5**, 285 (1990).
[23] N. C. Constantinou and B. K. Ridley, Phys. Rev. B **41**, 10 622 (1990).
[24] R. Enderlein, Phys. Rev. B **47**, 2162 (1993).
[25] P. A. Knipp and T. L. Reinecke, Phys. Rev. B **45**, 9091 (1992).
[26] W. Kim, M. A. Stroscio, A. Bhatt, R. Mickevicius, and V. V. Mitin, J. Appl. Phys. **70**, 319 (1991).
[27] R. Mickevicius, V. V. Mitin, K. W. Kim, M. A. Stroscio, and G. J. Iafrate, J. Phys. Condens. Matter **4**, 4959 (1992).
[28] P. A. Knipp and T. L. Reinecke, Phys. Rev. B **48**, 5700 (1993).
[29] S. Yu, K. W. Kim, M. A. Stroscio, G. J. Iafrate, and A. Ballato, Phys. Rev. B **50**, 1733 (1994).
[30] V. G. Grigoryan and D. G. Sedrakyan, Akust. Zh. **29**, 470 (1983) [Sov. Phys. Acoust. **29**, 281 (1983)].
[31] N. Nishiguchi, Phys. Rev. B **50**, 10 970 (1994).
[32] N. Nishiguchi (unpublished).

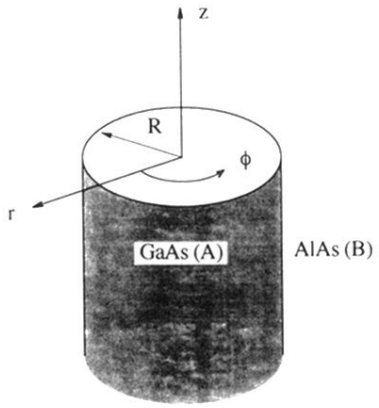

FIG. 1. Geometry of a cylindrical GaAs quantum wire surrounded by bulk AlAs.

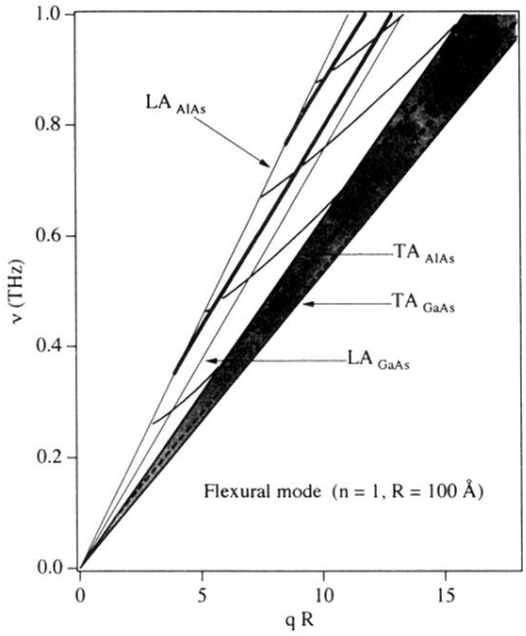

FIG. 12. Dispersions of the resonant flexural phonon modes in the frequency region $q\,v_{\mathrm{AlAs,TA}} < \omega < q\,v_{\mathrm{AlAs,LA}}$ for $R = 100$ Å. The thick and thin solid lines denote the dispersions of the quasiconfined and entirely extended resonant phonon modes, respectively. The dashed lines in the shaded region $q\,v_{\mathrm{GaAs,TA}} < \omega < q\,v_{\mathrm{AlAs,TA}}$ are the dispersions of the confined flexural phonon mode with $n = 1$.

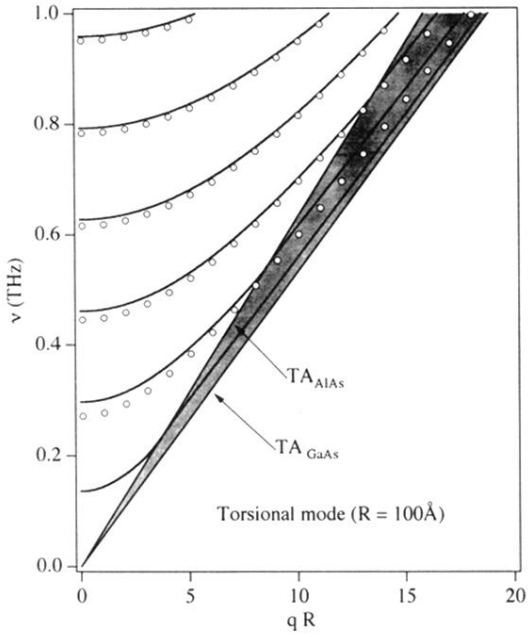

FIG. 4. Dispersions of the resonant torsional modes for $R = 100$ Å. The thick solid lines denote the dispersions and the thin lines in the shaded region between the bulk-TA_{GaAs} and -TA_{AlAs} dispersion curves are those of the confined torsional phonon mode (Ref. 31). The open circles denote the dispersions of the torsional phonon mode of a free-standing wire with the same radius.

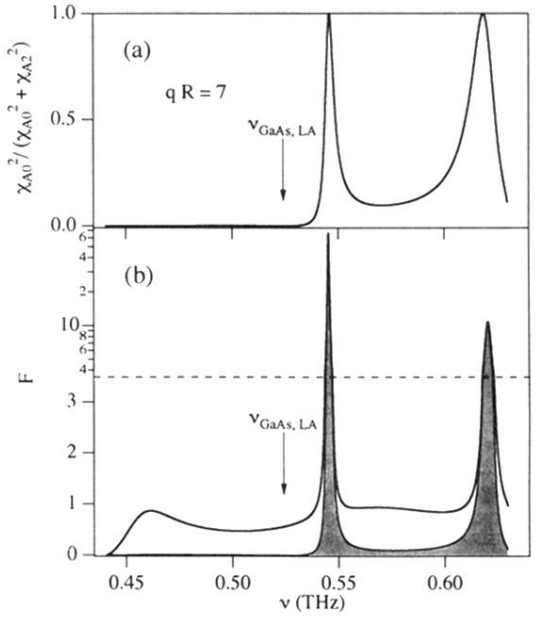

FIG. 7. (a) Contribution of the LA wave to the dilatational phonon mode versus frequency and (b) the corresponding F for $R = 100$ Å. The reduced longitudinal wave number is set at $qR = 7$. The shaded region in (b) denotes the F solely attributed to the LA wave in the wire. The dashed horizontal line in (b) denotes the change of scale from a linear to a logarithmic one.

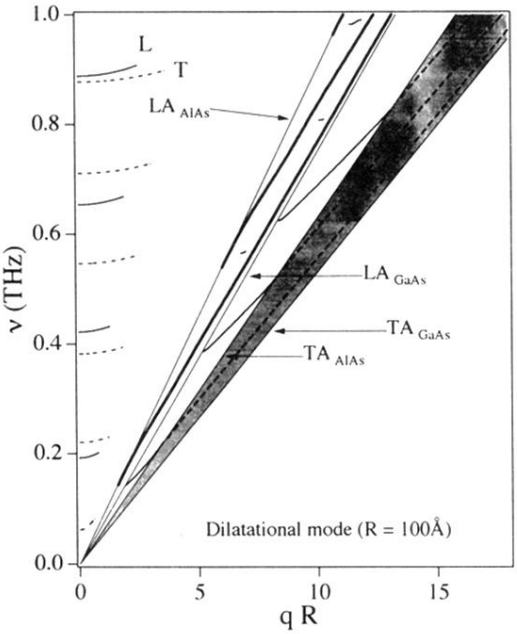

FIG. 8. Dispersions of the resonant dilatational phonon modes for $R = 100$ Å. The thick and thin solid lines in the frequency region $q\,v_{\mathrm{AlAs,TA}} < \omega < q\,v_{\mathrm{AlAs,LA}}$ denote the quasiconfined and entirely extended resonant modes, respectively. The dashed lines in the shaded region between the bulk-$\mathrm{TA_{GaAs}}$ and $\mathrm{TA_{AlAs}}$ dispersion curves are the dispersions of the confined dilatational modes (Ref. 31). The solid (L) and dashed (T) lines in the region $\omega > q v_{\mathrm{AlAs,LA}}$ are the dispersions of the entirely extended resonant modes attributed solely to the LA wave and TA wave in the wire, respectively.